Supplementary Materials

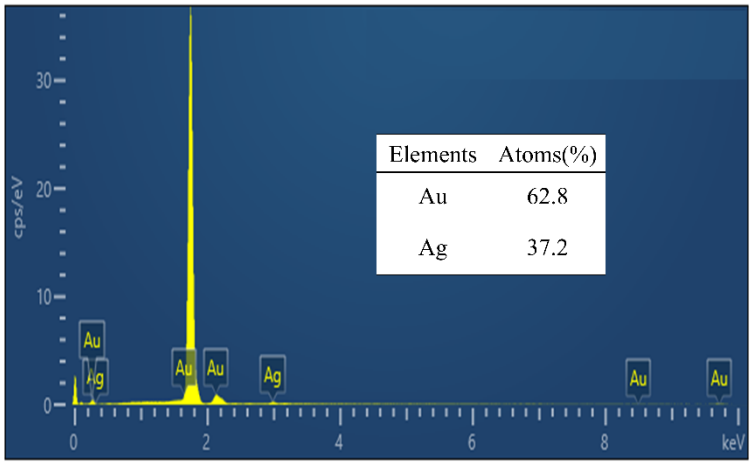
Microstructure regulation of hollow AuAg alloy nanobowls toward high-performance electrochemical urea biosensing

Tongtong Zhang[1,2,#], Zhijun Zou[1,2,#], Ruijin Meng[1,2], Songzhu Luo[3], Zhe Shen[2], Xiaofeng Zhu[1], Qiurong Lin[1], Jian Ma[2,4], Chao Jin[5], Zhen Li[2], Yu Zhang[6], Jinhu Yang[2,4], Wei Xu[1]

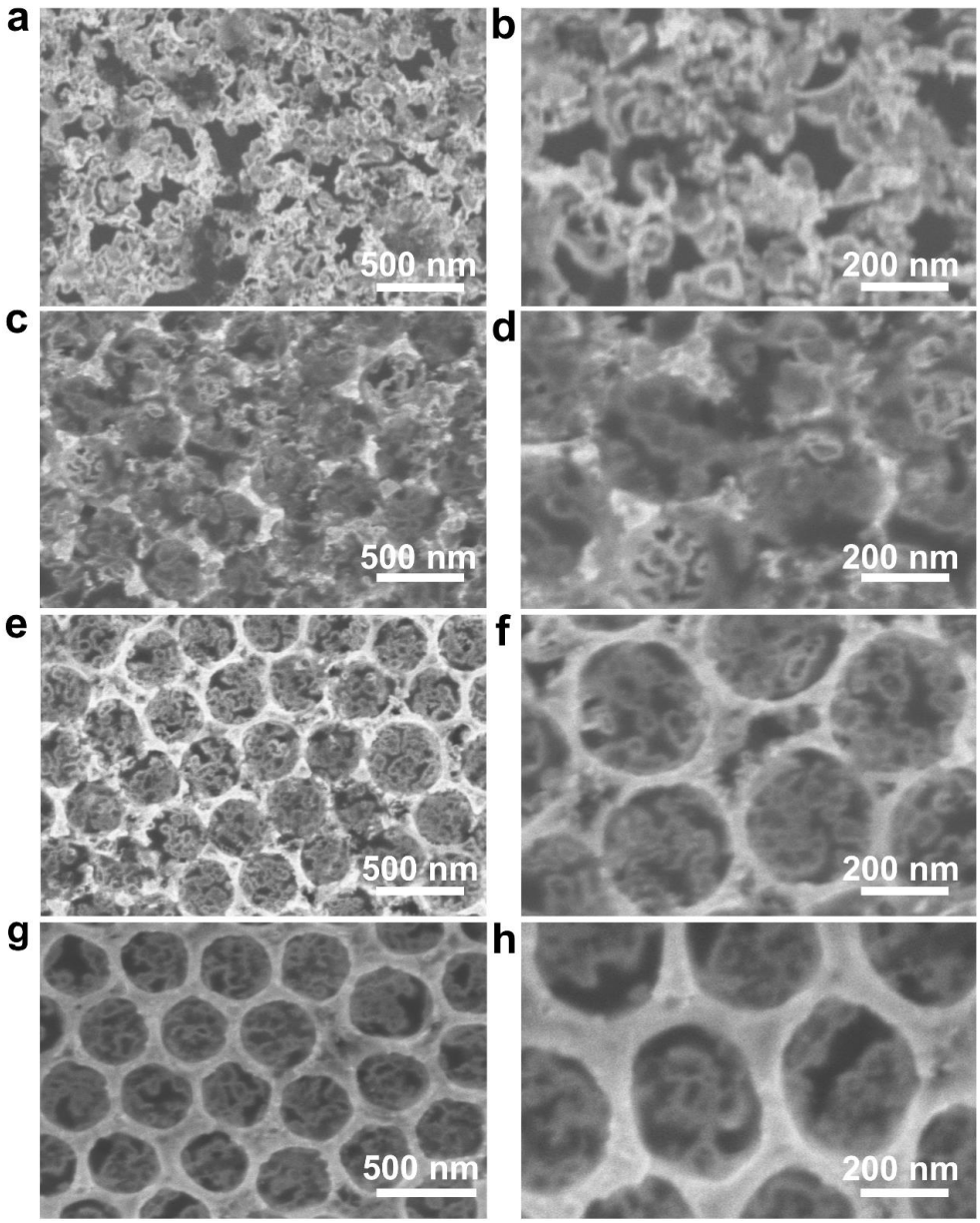
[1]Department of Optometry, Shanghai Eye Diseases Prevention & Treatment Center/Shanghai Eye Hospital, School of Medicine, Tongji University; National Clinical Research Center for Eye Diseases; Shanghai Engineering Research Center of Precise Diagnosis and Treatment of Eye Diseases; Eye Public Health Research Center, School of Medicine, Tongji University, Shanghai 200040, China.
[2]School of Chemical Science and Engineering, Tongji University, Shanghai 200092, China.
[3]Centre of High Field Nuclear Magnetic Resonance (NMR) Spectroscopy and Imaging, Nanyang Technological University, Singapore 637371, Singapore.
[4]College of Materials and Chemical Engineering, Fuyang University of Technology, Fuyang 236115, Anhui, China.
[5]Preservation and Conservation Center, Shanghai Library (Institute of Scientific and Technical Information of Shanghai), Shanghai 200031, China.
[6]School of Mechanical and Power Engineering, East China University of Science and Technology, Shanghai 200237, China.
[#]Authors contributed equally.

Correspondence to: Dr. Ruijin Meng, Department of Optometry, Shanghai Eye Diseases Prevention & Treatment Center/Shanghai Eye Hospital, School of Medicine, Tongji University; National Clinical Research Center for Eye Diseases; Shanghai Engineering Research Center of Precise Diagnosis and Treatment of Eye Diseases;

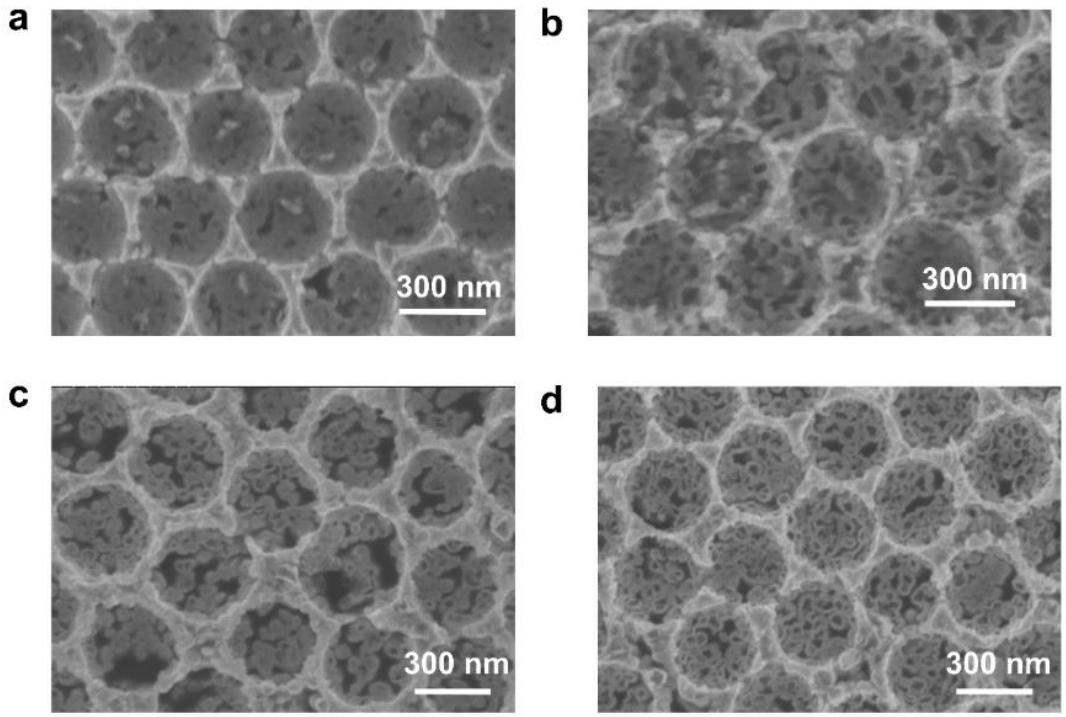
Eye Public Health Research Center, School of Medicine, Tongji University, Shanghai 200040, China; School of Chemical Science and Engineering, Tongji University, Shanghai 200092, China. E-mail: ruijinmeng@tongji.edu.cn; Prof. Yu Zhang, School of Mechanical and Power Engineering, East China University of Science and Technology, Shanghai 200237, China. E-mail: yzhang071@ecust.edu.cn; Prof. Jinhu Yang, School of Chemical Science and Engineering, Tongji University, Shanghai 200092, China; College of Materials and Chemical Engineering, Fuyang University of Technology, Fuyang 236115, Anhui, China. E-mail: yangjinhu@tongji.edu.cn; Dr. Wei Xu, Department of Optometry, Shanghai Eye Diseases Prevention & Treatment Center/Shanghai Eye Hospital, School of Medicine, Tongji University; National Clinical Research Center for Eye Diseases; Shanghai Engineering Research Center of Precise Diagnosis and Treatment of Eye Diseases; Eye Public Health Research Center, School of Medicine, Tongji University, Shanghai 200040, China. E-mail: 97778@tongji.edu.cn



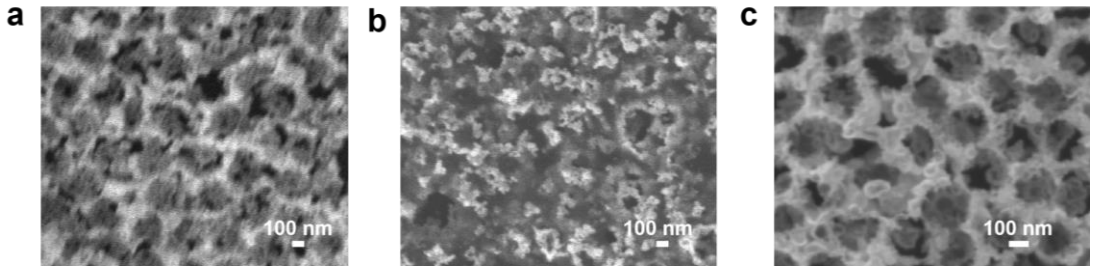
Supplementary Figure 1. EDS spectrum of the AuAg NBs. The inset shows the atomic percentages values of Au and Ag.



Supplementary Figure 2. SEM images of AuAg NBs prepared at different Na_2HPO_4 concentrations. (a, b) 10 mM, (c, d) 50 mM, (e, f) 75 mM, and (g, h) 150 mM. The concentration of $HAuCl_4$ was fixed at 3 mM.



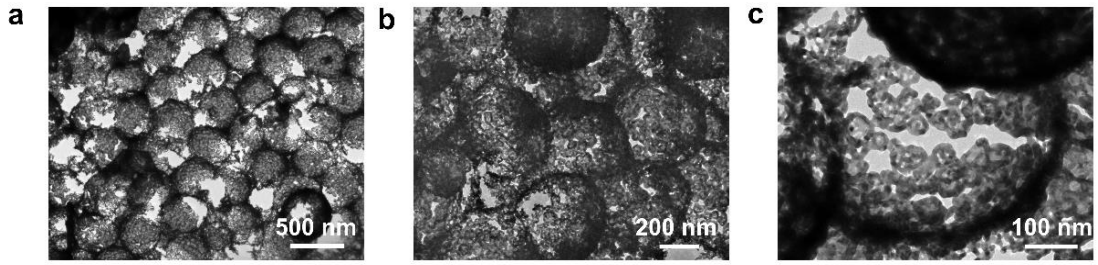
Supplementary Figure 3. SEM images of AuAg NBs prepared at different Na_2HPO_4 concentrations: (a) 1 mM, (b) 2.5 mM, (c) 5 mM, and (d) 7.5 mM. The concentration of $HAuCl_4$ was fixed at 0.3 mM.



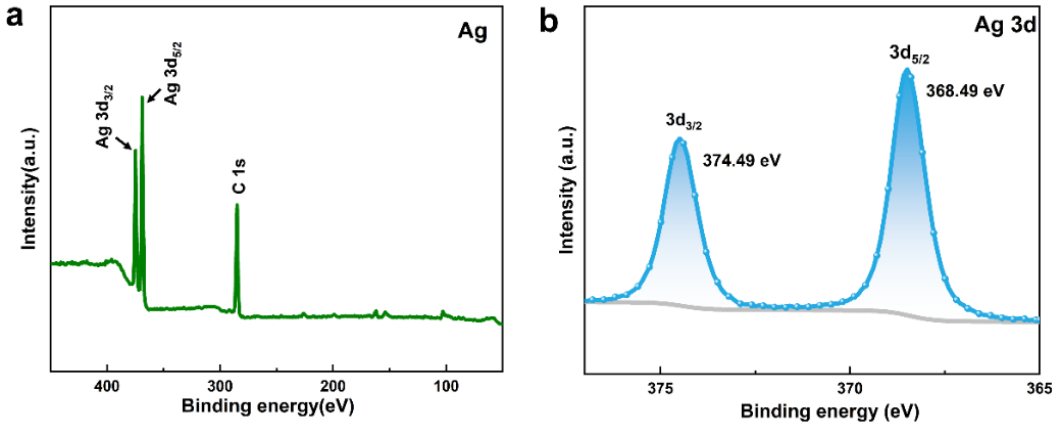
Supplementary Figure 4. SEM images of AuAg NBs synthesized at 0 °C (a) and 60 °C (b), and using NaOH as a substitute for Na_2HPO_4 (c), respectively.

Note: Reaction kinetics also showed a pronounced influence on the structural evolution. For the temperature-dependent experiments, the reaction solution contained 3 mM $HAuCl_4$ and 150 mM Na_2HPO_4 in both cases, with the reaction temperature varied to 0 and 60 °C. At 0 °C, the products retained some pore- and bowl-like features, but the nanobowl boundaries were indistinct and the hierarchical nesting of small nanobowls within larger ones was poorly developed (Supplementary Figure 4a).

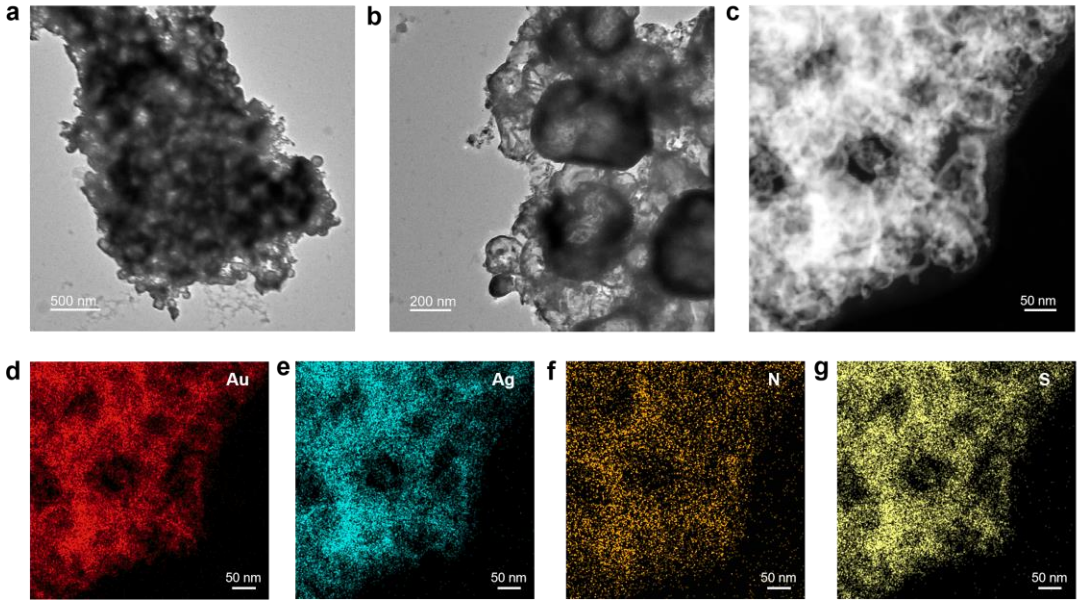
By contrast, at 60 °C, the hierarchical structure was severely disrupted, with the large nanobowl structures disappearing and the overall arrangement becoming disordered (Supplementary Figure 4b). Such temperature-dependent changes indicate that either excessively slow or excessively rapid galvanic replacement is unfavorable for the development of a well-defined hierarchical architecture. In a separate control experiment, NaOH was used instead of Na_2HPO_4, and the pH of the reaction solution was adjusted to the same value as that of the solution containing 3 mM $HAuCl_4$ and 150 mM Na_2HPO_4. Under this condition, an ordered hierarchical morphology in which small nanobowls were nested within larger nanobowls was still obtained (Supplementary Figure 4c). This observation suggests that the morphology-regulating role of Na_2HPO_4 is mainly associated with its effect on the alkalinity of the reaction solution rather than with a phosphate-specific effect. Overall, Na_2HPO_4 appears to regulate the formation of hierarchical AuAg NBs primarily by adjusting the solution pH and thereby modulating the kinetics of the galvanic replacement reaction. An appropriate reaction rate is therefore essential for obtaining a well-defined hierarchical nanobowl structure. Based on these observations, 3 mM $HAuCl_4$ and 150 mM Na_2HPO_4 at room temperature were selected as the optimized reaction conditions for the subsequent experiments.



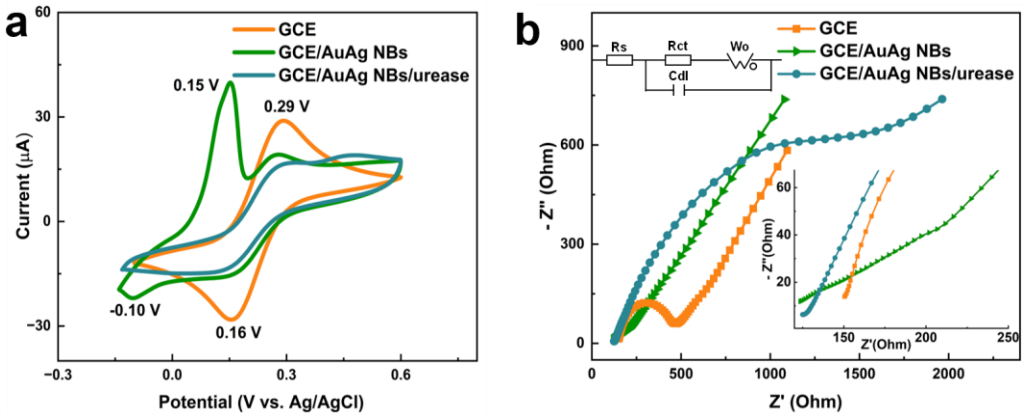
Supplementary Figure 5. TEM images of AuAg NBs at different magnifications: (a) low-magnification (scale bar: 500 nm); (b) medium-magnification (scale bar: 200 nm); (c) high-magnification (scale bar: 100 nm).



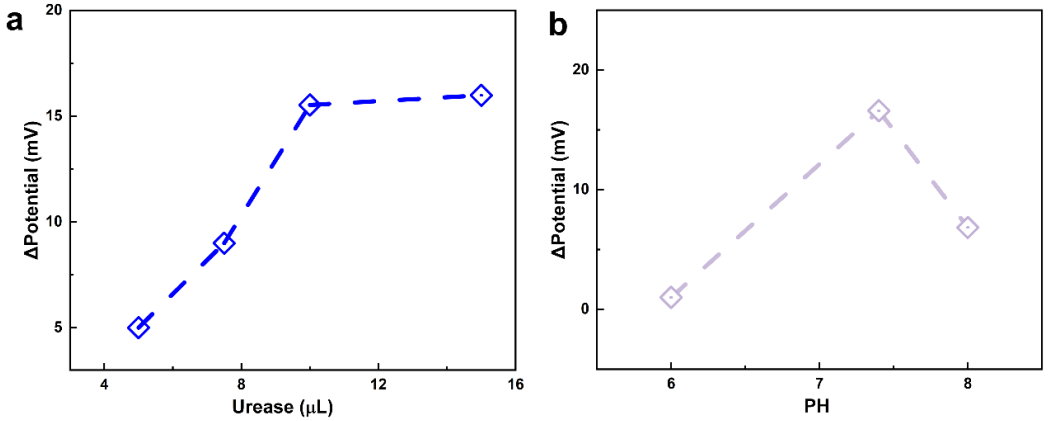
Supplementary Figure 6. XPS spectra of Ag film. (a) Survey spectrum and (b) high-resolution Ag 3d spectrum.



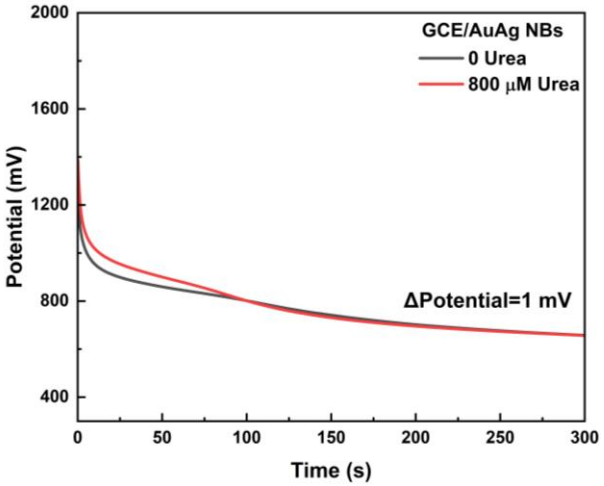
Supplementary Figure 7. (a,b) TEM images of AuAg NBs after urease immobilization. (c) STEM image and corresponding EDS elemental maps of (d) Au, (e) Ag, (f) N and (g) S.



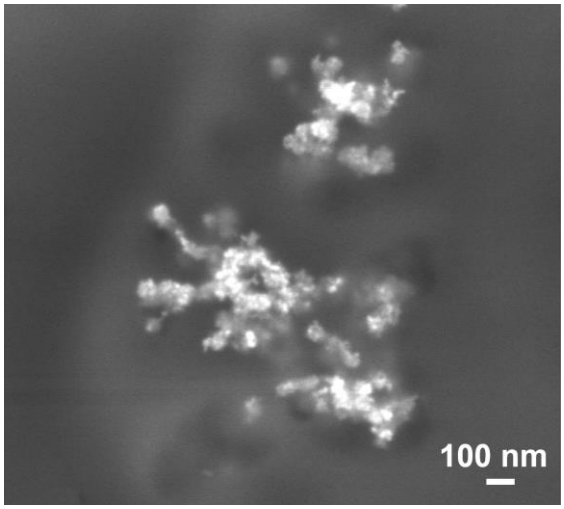
Supplementary Figure 8. (a) CV, (b) EIS curves of the GCE, GCE/AuAg NBs and GCE/AuAg NBs/urease electrodes.



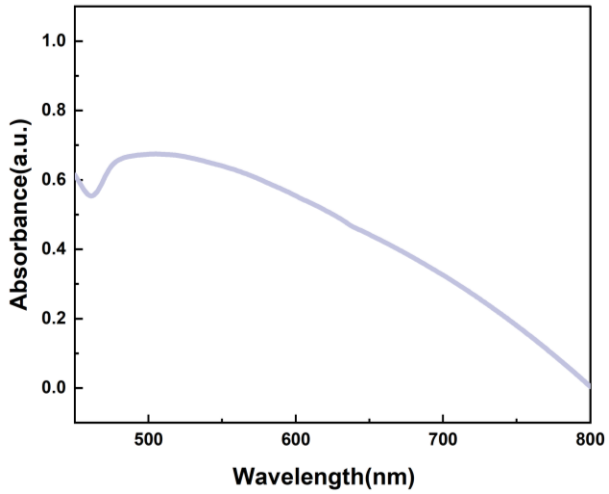
Supplementary Figure 9. Potentiometric responses of the GCE/AuAg NBs/urease electrode to 800 μM urea at different (a) urease loading volumes (5, 7.5, 10 and 15 μL) and (b) pH values (6, 7.4 and 8).



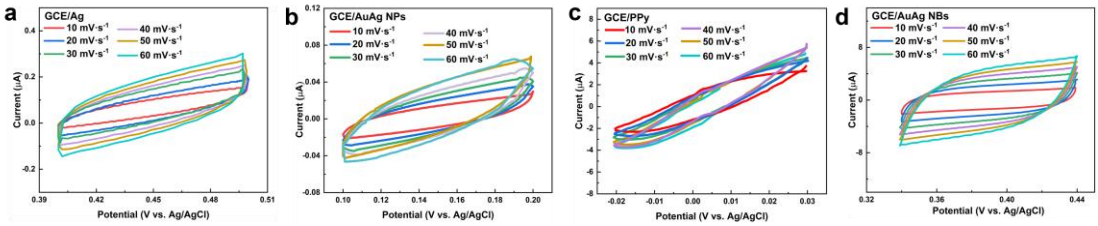
Supplementary Figure 10. Potentiometric response of the GCE/AuAg NBs electrode to 800 μM urea.



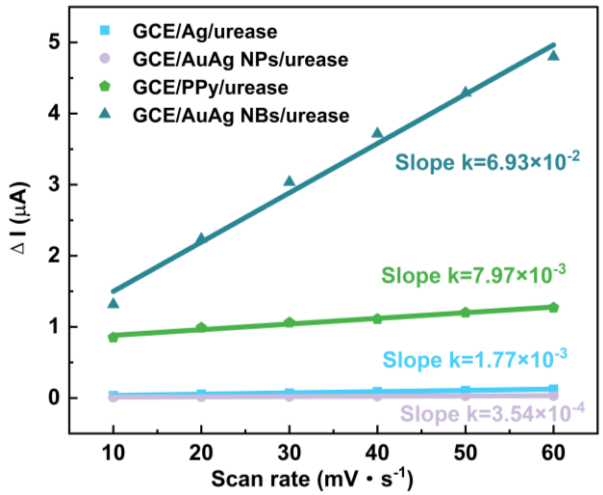
Supplementary Figure 11. SEM image of AuAg NPs.



Supplementary Figure 12. UV-vis spectrum of AuAg NPs.

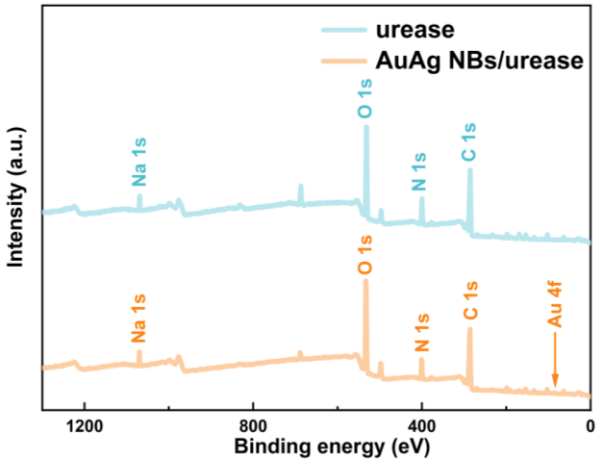


Supplementary Figure 13. CV curves of (a) GCE/Ag, (b) GCE/AuAg NPs, (c) GCE/PPy, and (d) GCE/AuAg NBs at different scan rates.

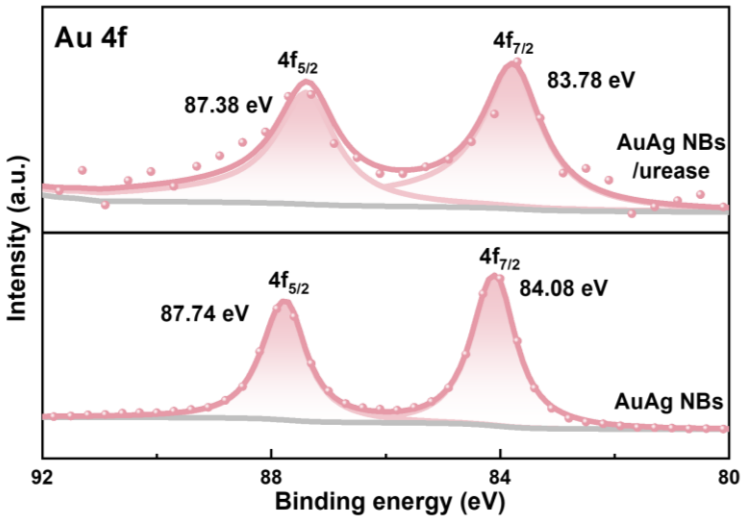


Supplementary Figure 14. Linear plots of capacitive current ΔI versus scan rate for GCE/Ag, GCE/AuAg NPs, GCE/PPy and GCE/AuAg NBs.

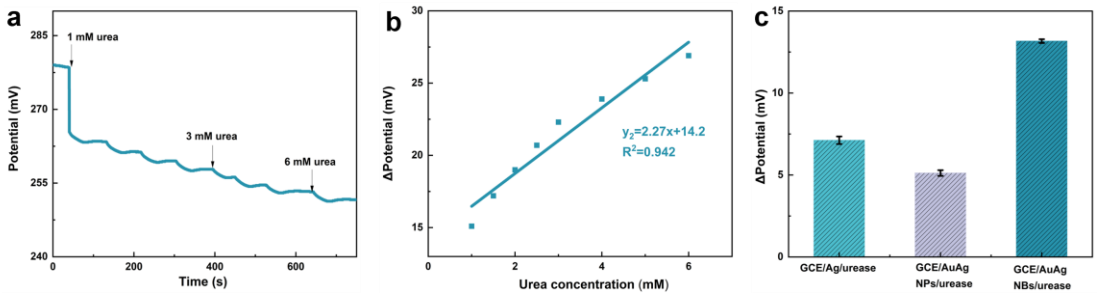
Note: This estimation assumes that the current in the selected non-Faradaic region is dominated by double-layer charging, that the capacitive current varies approximately linearly with scan rate, and that the selected C_s values reasonably represent the corresponding electrode interfaces[1]. For GCE/Ag, GCE/AuAg NPs, and GCE/AuAg NBs, a common specific capacitance C_s of 20 μF cm^{-2} was adopted to ensure consistency in comparing these three precious-metal-based electrodes, using a value commonly reported in the literature as an approximation for smooth metal surfaces[2]. For GCE/PPy, a C_s value of 40 μF cm^{-2} was adopted as a reference based on a previous study of a PPy@Co_3O_4 composite catalyst[3]. As C_s depends on surface composition, morphology, and experimental conditions, the adopted values are literature-based approximations rather than experimentally determined parameters specific to our electrodes. Accordingly, the calculated ECSA values should be regarded as rough estimates for semi-quantitative comparison.



Supplementary Figure 15. XPS survey spectra of urease and AuAg NBs/urease**.**



Supplementary Figure 16. High-resolution Au 4f spectra of AuAg NBs/urease and AuAg NBs.

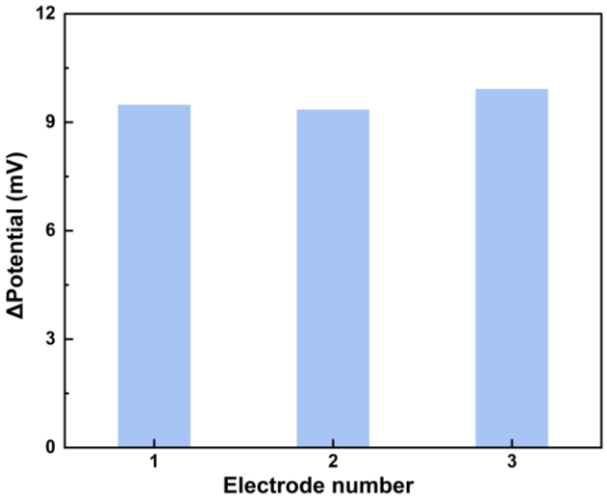


Supplementary Figure 17. (a) Potentiometric response of the GCE/AuAg NBs/urease electrode with increasing urea concentration from 1 to 6 mM. (b) Calibration curve derived from panel (a). (c) Potentiometric responses of different electrodes to 2 mM urea (SD of n = 3).

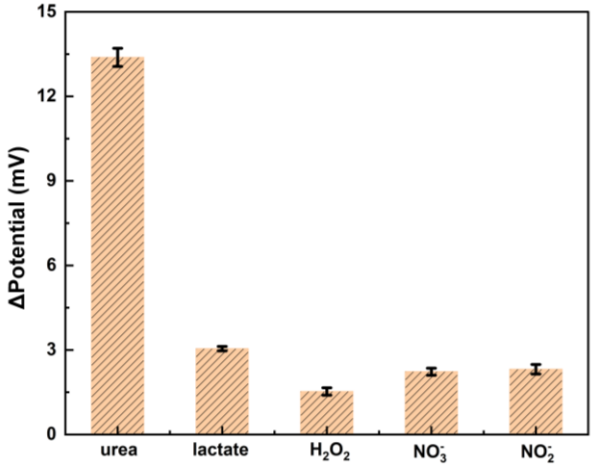
Note: LOD was calculated as follows:

LOD = 3σ/S

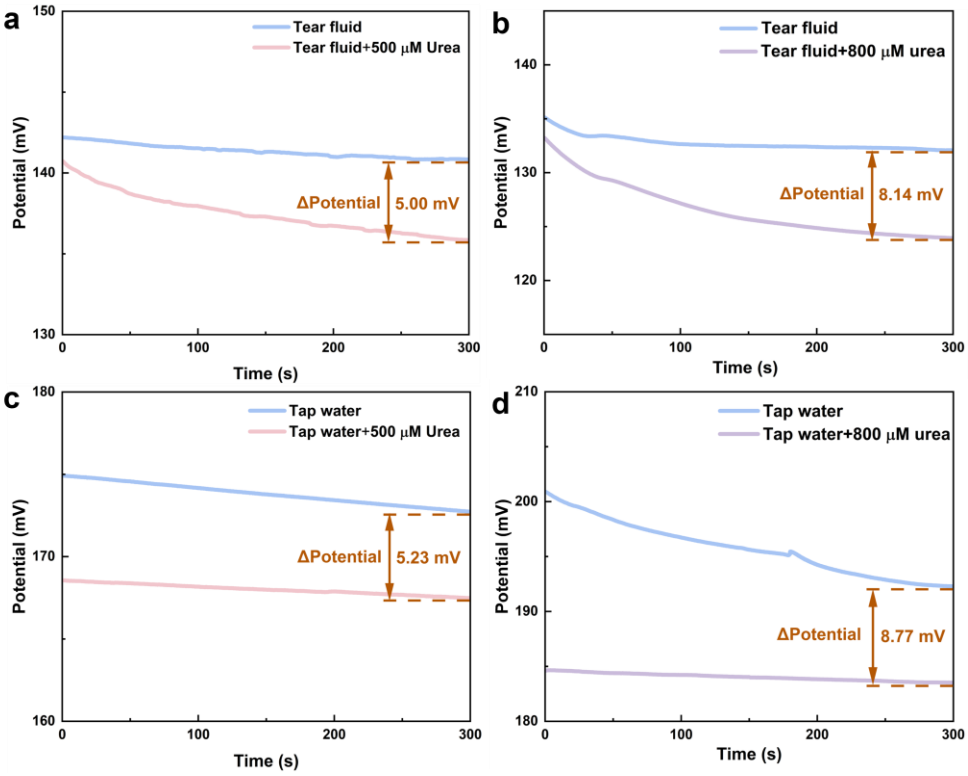
where σ represents the standard deviation of the blank responses and S is the slope of the corresponding calibration curve. The standard deviations were 0.0237 mV and 0.0235 mV for the GCE/AuAg NBs/urease and SPCE/AuAg NBs/urease, respectively.



Supplementary Figure 18. Batch-to-batch reproducibility of three independently prepared GCE/AuAg NBs/urease electrodes toward 800 μM urea.



Supplementary Figure 19. Interference study using 2 mM lactate, 0.1 mM H_2O_2, 10 μM NO_3^- and 2 μM NO_2^- in addition to 2 mM urea (SD of n = 3).



Supplementary Figure 20. Potentiometric responses for urea detection in (a, b) tear fluid and (c, d) tap water.

Supplementary Table 1. pH of the reaction solutions at different Na_2HPO_4 concentrations

Na_2HPO_4 concentration (mM)	150	75	50	10
pH	9.12	8.75	8.58	7.4

Supplementary Table 2. Rs and Rct Values for GCE, GCE/AuAg NBs and GCE/AuAg NBs/urease

Electrode	**Rs (Ω)**	**Rct (Ω)**
GCE	152.7	180.8
GCE/AuAg NBs	119.7	26.14
GCE/AuAg NBs/urease	140.7	1155

Supplementary Table 3. Response times of sensors under different experimental conditions

Electrode	Electrode area (mm^2)	Urease loading (μL)	pH	Stirring speed (rpm)	*t*90 (s)
GCE/AuAg NBs/urease	7	5	7.4	0	265.5
GCE/AuAg NBs/urease	7	7.5	7.4	0	220.5
GCE/AuAg NBs/urease	7	15	7.4	0	262.5
GCE/AuAg NBs/urease	7	10	6	0	250.0
GCE/AuAg NBs/urease	7	10	8	0	244.5
GCE/AuAg NBs/urease	7	10	7.4	500	136.0
SPCE/AuAg NBs/urease	28	10	7.4	0	225.0

Supplementary Table 4. Comparison of the potentiometric responses of the GCE/AuAg NBs/urease sensor in diluted and undiluted artificial tear samples

Urea concentration (μM)		500	800
Potential response (mV)	Undiluted artificial tears	4.71	8.51
	Diluted artificial tears	5.00	8.14

Supplementary Table 5. GCE/AuAg NBs/urease electrode response to urea in real samples

Samples	Spiked (μM)	Found (μM)	Recovery (%)
tear fluid	500	469	93.8
	800	765	95.7
tap water	500	491	98.2
	800	825	103.0

Supplementary Table 6. Comparison of the urea detection performance of GCE/AuAg NBs/urease and some reported sensing systems

Electrode	Sensing principle	Method of detection	Linear range (mM)	LOD (μM)	Stability (days)	Sample matrix	pH	Temperature (°C)	Response time (s)	Reference
Ni@NiMn	Non-enzymatic	cyclic voltammetry	1-9	18.7	-	human blood	14	20	-	[4]
MNA-MC[a]	Enzymatic	potentiometry	3-18	900	10	ISF[h]	-	37	-	[5]
PVdF[b]/Ni−Co(0.5:0.5)	Non-enzymatic	amperometry	0.02-2	12	30	human urine	14	-	5	[6]
urease/SF[c]/aminated GCE	Enzymatic	cyclic voltammetry	0.3-2.7	163	-	PBS[i]	7	-	60	[7]
integrated tip-like sensor	Enzymatic	voltammetry	0.5−7	20	-	human urine	4-8	-	600	[8]

f-GNPlts[d]/GNDs[e]/urease	Enzymatic	current voltage	1.6-15	83	15	milk	7	-	20	[9]
MoS_2 QDs[f]/Urs[g]/SF[c]/NH_2–GCE	Enzymatic	cyclic voltammetry	0.1-1.9	274	10	PBS[i]	7	-	560	[10]
GCE/Au Ag NBs/urease	Enzymatic	potentiometry	0.1-1/1-6	6.7	15	AT[j]	7.4	25	207.5	this work

[a] MNA-MC: microneedle array-microcavities; [b] PVdF: polyvinylidene fluoride; [c] SF: silk fibroin; [d] f-GNPlts: functionalized graphene nanoplatelet; [e]GNDs: graphitized nanodiamond; [f]QDs: quantum dots; [g]Urs: urease; [h]ISF: interstitial fluid; [i]PBS: phosphate buffer solution; [j]AT: artificial tears

REFERENCES

1. Morales, D. M.; Risch, M. Seven steps to reliable cyclic voltammetry measurements for the determination of double layer capacitance. *J. Phys.: Energy*. **2021**, *3*, 034013. DOI: 10.1088/2515-7655/abee33

2. Bi, J.; Li, P.; Liu, J.; Jia, S.; Wang, Y.; Zhu, Q.; Liu, Z.; Han, B. Construction of 3D copper-chitosan-gas diffusion layer electrode for highly efficient CO_2 electrolysis to C_{2+} alcohols. *Nature Communications*. **2023**, *14*, 2823. DOI: 10.1038/s41467-023-38524-3

3. Ai, H.; Fan, L.; Wang, Y.; Wang, Z.; Zhang, H.; Zhao, J.; Jiao, M.; Lv, B.; Han, X. OER catalytic performance of a composite catalyst comprising multi-layer thin flake Co_3O_4 and PPy nanofibers. *RSC Adv.* **2023**, *13*, 32045-32053. DOI: 10.1039/d3ra05936g

4. Ezzat, N.; Hefnawy, M. A.; Fadlallah, S. A.; El-Sherif, R. M.; Medany, S. S. Synthesis of nickel-sphere coated Ni-Mn layer for efficient electrochemical detection of urea. *Sci. Rep.* **2024**, *14*, 14818. DOI: 10.1038/s41598-024-64707-z

5. Dervisevic, M.; Jara Fornerod, M. J.; Harberts, J.; Zangabad, P. S.; Voelcker, N. H. Wearable microneedle patch for transdermal electrochemical monitoring of urea in interstitial fluid. *ACS Sens.* **2024**, *9*, 932-941. DOI: 10.1021/acssensors.3c02386

6. Babu, K. J.; Senthilkumar, N.; Kim, A. R.; kumar, G. G. Freestanding and binder free PVdF-HFP/Ni-Co nanofiber membrane as a versatile platform for the electrocatalytic oxidation and non-enzymatic detection of urea. *Sens. Actuators, B.* **2017**, *241*, 541-551. DOI: 10.1016/j.snb.2016.10.069

7. Rafiq, K.; Mai, H. D.; Kim, J. K.; Woo, J. M.; Moon, B. M.; Park, C. H.; Yoo, H. Fabrication of a highly effective electrochemical urea sensing platform based on urease-immobilized silk fibroin scaffold and aminated glassy carbon electrode. *Sens. Actuators, B.* **2017**, *251*, 472-480. DOI: 10.1016/j.snb.2017.05.048

8. Liu, J.; Lu, W.; Zhang, L.; Yang, J.; Yao, Z.-P.; He, Y.; Li, Y. Integrated hand-held electrochemical sensor for multicomponent detection in urine. *Biosens. Bioelectron.* **2021**, *193*, 113534. DOI: 10.1016/j.bios.2021.113534

9. Kumar, V.; Kaur, I.; Arora, S.; Mehla, R.; Vellingiri, K.; Kim, K.-H. Graphene

nanoplatelet/graphitized nanodiamond-based nanocomposite for mediator-free electrochemical sensing of urea. *Food Chem.* **2020**, *303*, 125375. DOI: 10.1016/j.foodchem.2019.125375

10. Sadia, I.; Rafiq, K.; Abid, M. Z.; Jalil, M.; Javed, R.; Rauf, A.; Hussain, E. Unraveling the potential and selectivity of MoS_2 quantum dots for enzyme-based electrochemical detection of urea. *ACS Appl. Nano Mater.* **2025**, *8*, 19929-19942. DOI: 10.1021/acsanm.5c03505